STATISTICAL PROCESS CONTROL OF COMMERCIAL FORCE-SENSING RESISTORS

Carlos Andrés Palacio Gómez[1], Leonel Paredes-Madrid[2], Andrés Orlando Garzon[2]

1) *GIFAM Group, Universidad Antonio Nariño, Cra 7 No. 21-84, 150001 Tunja, Boyacá, Colombia* (*carlospalacio@uan.edu.co*)

2) *Universidad Católica de Colombia, Faculty of Engineering, Carrera 13 # 47 – 30, Bogota, Colombia* (✉ *ljparedes@ucatolica.edu.co*, *aogarzon@ucatolica.edu.co*, +57 601 327 73 00).

Abstract

The manufacturing and characterization of polymer nanocomposites is an active research trend nowadays. Nonetheless, statistical studies of polymer nanocomposites are not an easy task since they require several factors to consider, such as: large amount of samples manufactured from a standardized procedure and specialized equipment to address characterization tests in a repeatable fashion. In this manuscript, the experimental characterization of sensitivity, hysteresis error and drift error was carried out at multiple input voltages (U_s) for the following commercial brands of FSRs (*force sensing resistors*): Interlink FSR402 and Peratech SP200-10 sensors. The quotient between the mean and the standard deviation was used to determine dispersion in the aforementioned metrics. It was found that a low mean value in an error metric is typically accompanied by a comparatively larger dispersion, and similarly, a large mean value for a given metric resulted in lower dispersion; this observation was held for both sensor brands under the entire range of input voltages. In regard to sensitivity, both sensors showed similar dispersion in sensitivity for the whole range of input voltages. Sensors' characterization was carried out in a tailored test bench capable of handling up to 16 sensors simultaneously; this let us speed up the characterization process.

Keywords: force sensing resistors (FSR), pressure sensor, statistical process control, hysteresis error, drift error.

1. Introduction

Polymer nanocomposites have gained great attention in recent years due to multiple front–end applications that have been developed. Besides the traditional applications of strain and stress sensing [1–4], polymer nanocomposites have also found acceptance in chemical and pollutant sensing, *e.g.* Fernandez *et al.* have successfully developed ammonia sensors through the combination of polypyrrole with other polymers [5]. Similarly, Lu *et al.* have developed composite materials capable of measuring chemical vapours of dimethylformamide, ammonia, and physical variables such as temperature and strain [6]; this kind of multi-variable sensor was developed through the combination of graphite nanosheets with polyamide. Other studies reporting the usage of nanocomposites for vapour and gas sensing can be found in the review article from Shukla and Saxena [7]. The main benefits of polymer nanocomposites over other sensing solutions can be explained with the ease of manufacturing, low cost and high availability of polymers and fillers [8].

Despite multiple studies reporting polymer nanocomposites and their applications [8–11], only few studies have embraced a statistical approach to evaluate the performance of polymer nanocomposites. More specifically, statistical tools have been primarily employed to study the

effect of a design parameter on sensor's sensitivity, but they have not been extensively used to assess the statistical distribution of hysteresis, drift and other error metrics. To exemplify this, we can mention the studies from Saleh *et al.* [12], and Yuan and Lin [13]. Saleh *et al.* embraced T-Tests to study the effect of either using polylactic acid or polyurethane to assemble health monitoring sensors [12]. Likewise, Yuan and Lin used tools from *Principal Component Analysis* (PCA) to identify interactions of ammonia and chloroform with nanocomposites manufactured from multiple polymers and *Carbon Nanotubes* (CNTs) [13]. Similar approaches have been reported in the studies from Speller *et al.* [14], and Jaffal *et al.* [15].

Following the previous statement, a great effort has been also placed on the manufacturing of aerogels comprising carbon nanofibers and conductive polymers as means of strain sensing [16], [17]. Similarly, multiple authors have explored nanocomposites with multiple fillers to enhance sensor performance [18], [19], and more recently, self–healing properties have been incorporated to stress/strain sensors [20], [21]. On the other hand, only few studies have employed statistical tools to comparatively analyse the performance metrics of polymer nanocomposites aimed for stress/strain sensing; this is the case of the studies by Hall *et al.* [22], Komi *et al.* [23], Dabling *et al.* [24], and Hollinger and Wanderley [25]. Nonetheless, such studies have mostly embraced a reduced number of sensors in the assessment of the following performance metrics: hysteresis error, drift error, repeatability error and sensitivity degradation. Naturally, a reduced number of sensors cannot provide us with an adequate framework for statistical analysis, and for this reason, a different approach was taken up in this research.

We can only hypothesize possible reasons that keep researchers away from statistical studies in polymer nanocomposites. Considering that statistical studies require large sample counts, cost and manufacturing time are major factors to consider. However, according to the authors' criteria, the most powerful reason is the inability of most research labs to manufacture and test large amounts of sensors following a standardized procedure. Depending on the methodology used, it is requires between 40 and 100 specimens to obtain statistically representative results; these quantities may not seem too large from a manufacturing standpoint, but during testing and characterization, these quantities are simply too large because most research labs are equipped with one-specimen measuring equipment. Moreover, some test protocols involve settling times of nearly one hour which dramatically increases the length of the characterization process.

Based on previous observations, this study comprised the statistical characterization of two commercial brands of *Force Sensing Resistors* (FSRs) manufactured from a blend of insulating polymer and carbon black. The sensors chosen for this study were: Interlink FSR402, manufactured by Interlink Electronics, Inc. (Westlake Village, CA, USA) and Peratech SP200-10, manufactured by Peratech Holdco Limited (Sedgefield, UK). The characterization involved sensitivity, hysteresis and drift tests. In order to overcome the requirements of a lengthy characterization, a tailored test bench has been designed and built which is capable of handling up to 16 sensors simultaneously. With the aim of obtaining statistically representative results, a total of 48 specimens from each brand were evaluated; this let us assess not only the average of a given performance metric, but also its dispersion.

The rest of this paper is organized as follows: the experimental setup and characterization procedure is presented in Section 2, followed by the experimental results and discussion in Section 3. Finally, conclusions are stated in Section 4.

2. Experimental setup and characterization procedure

The entire characterization procedure was done with a tailored test bench capable of handling up to 16 sensors simultaneously using a sandwich-like configuration, see Fig. 1. Forces were applied from a linear stepper motor model L5918L3008, manufactured by Nanotec Electronic GmbH & Co (Feldkirchen, Germany). An LCHD-05 load cell manufactured by Omega Engineering, Inc. (Norwalk, CT, USA) was employed to close the force loop. Mechanical compliance was provided by a spring. Given the fact that lower sensors were more heavily loaded than on-top sensors, the error metrics from later sections took such a difference into account; this had a negligible impact on full sensor loading. However, in regard to the null-force condition, a clarification is required. The uppermost and lowermost sensors had the null-force loading of 0.49 N and 0.96 N, respectively. In the worst case scenario, the null-force loading represented only 4.8 % of FSRs' nominal capacity rated at 20 N; therefore, we could state that the sandwich-like configuration from Fig. 1 was a valid setup to speed up the characterization process with little effect on the performance metrics.
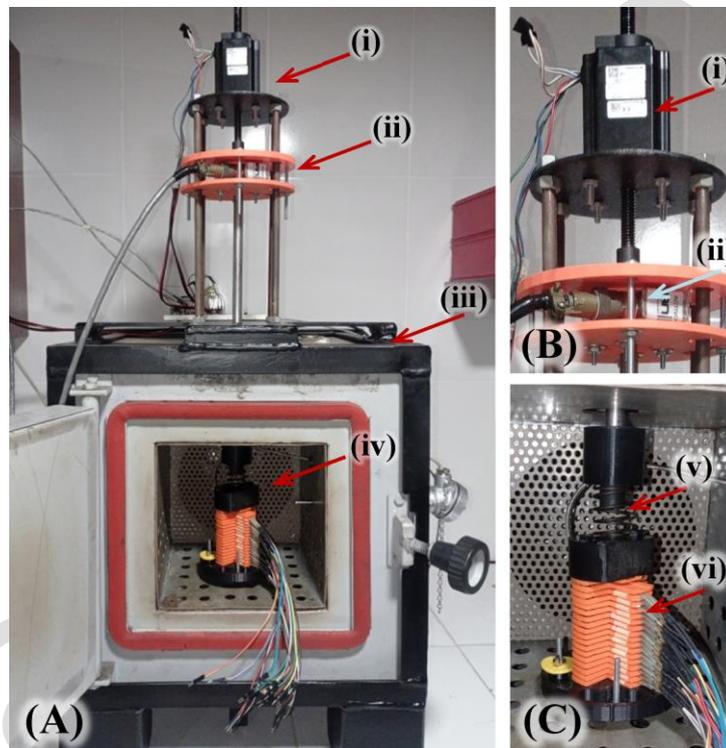

Fig. 1. Test bench for handling up to sixteen sensors simultaneously. (A) Overview of the testbench, the forces were applied with the linear motor (i) on-top of the arrangement, and the force loop was closed using the load cell (ii). The temperature chamber (iii) provided mechanical support to the structure and held temperature constant at 25ºC along the tests. Bunch of commercial Force Sensing Resistors (FSRs) (iv). (B) Close-up view of the linear motor and the load cell. (C) Sandwich-like configuration for handling the sensors, the spring (v) provided mechanical compliance to the arrangement of FSRs (vi).

The control scheme of the testbench is summarized in Fig. 2 (top). A digital Proportional Integral controller, $PI(z)$, was implemented to match the reference force (F_r) with the force measured at the bunch of sensors (F_o). The $PI(z)$ was implemented in LabVIEW using a cRIO-9035 Real-Time embedded controller. It must be emphasized that $PI(z)$ was tuned to avoid overshoot; this was required because FSRs exhibit considerable amounts of hysteresis that causes a non-linear variation in their output. Given the resolution of the stepper motor and the spring constant, the minimal force increment was set to 10 mN with a bandwidth of roughly 2 Hz; this frequency bandwidth was more than enough to apply the force profiles of

the experimental characterization. In fact, the system bandwidth was limited to 1 Hz by the analog multiplexer circuit of Fig. 3, and not by mechanical constraints of the testbench.
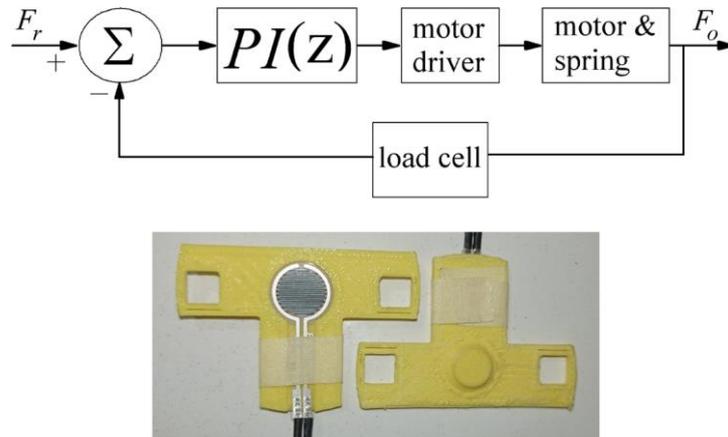

Fig. 2. (top) Sketch of the control force loop. (bottom) Top and bottom view of individual sensor holders.

According to thevsensors' datasheet, the Interlink FSR 402 and the Peratech SP200-10 sensors have the nominal capacities of 20 N [26], [27]. Both sensors have a continuous output meaning that a small increment in force and/or input voltage causes a variation in sensor's resistance; this has been demonstrated by our previous studies [28] and by third authors as well [23], [29]. The continuous output of both FSRs implies that sensors' sensitivity and performance metrics are influenced by the input voltage. Therefore, we require a driving circuit that lets us control the voltage across the sensors at any time; this can be achieved by means of an amplifier in inverting configuration, see Fig. 3. The low noise amplifier model OP470 was chosen for this purpose.

In order to enable readings from multiple sensors, a time-multiplexed circuit was implemented on the basis of the analog multiplexer model ADG444, see Fig. 3. A total of four ADG444 were incorporated, each with four analog inputs, thus enabling us to handle up to sixteen FSRs. Given the low on-resistance of the multiplexer (around 70 Ω), the error introduced by the mux could be neglected. A feedback resistor (R_f) of 510 Ω was chosen for all the tests with a tolerance of 1%. Given the input voltage (U_s), each sensor was activated accordingly to be sourced with U_s, and mechanically loaded with the intended force profile, *i.e.* with F_r in Fig. 2.

Three different force profiles were explored to assess the sensors' sensitivity and the performance metrics of hysteresis and drift; the protocols are next described:
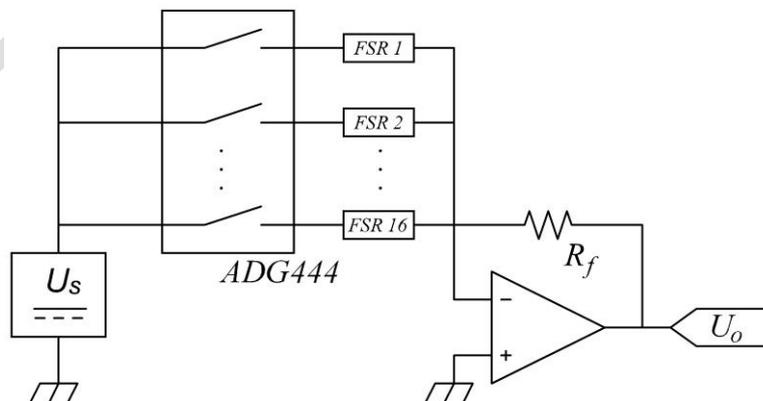

Fig. 3. Schematic of the driving circuit to handle up to sixteen FSRs on a time-multiplexed basis using the ADG444 analog mux. The driving voltage (Us) was changed along the characterization tests. The feedback resistor was set to 510 Ω for all the tests.

2.1. Sensitivity Characterization and General Considerations

The bunch of sensors were loaded in step increments of 1 N starting at null-input force up to the sensors' nominal range at 20 N. Later, we performed regression analysis to obtain the sensitivity of each sensor. The amplifier output voltage (U_o) was set as the system output, thanks to which we obtained a linear relationship between the applied force and U_o; this has been previously reported in literature [22], [23]. This procedure was repeated at the following input voltages, U_s: 0.25 V, 0.5 V, 0.75 V, 1 V. For voltages larger than 1 V, step increments of 0.5 V were applied up to 8.5 V. Therefore, a total of 19 different voltages were applied to the 48 specimens of each sensor brand.

The piezoresistive response of FSRs originates from two different phenomena: quantum tunnelling occurring in neighbouring particles, and constriction resistance occurring in particles in contact. This model was derived by Kalantari *et al.* [30] and was also demonstrated by the authors [31]. Both quantum tunnelling and constriction resistances are reduced for incremental forces, however, the former is heavily influenced by the input voltage [32], whereas the latter is not [33]. this has the ultimate consequence *i.e.* performance metrics are influenced by U_s. For this reason, we performed the sensors' characterization at multiple voltages.

2.2. Hysteresis Characterization

In order to determine the hysteresis error (*HE*), the following force profile was applied to the bunch of sensors: null-input force, half-nominal range ($U_o\_loading$ (10 N)), full sensor loading (U_o (20 N)), and then back to the half-nominal range ($U_o\_unloading$ (10 N)); this procedure was repeated at the input voltages specified in Section 2.1 for all the sensors. Finally, the Hysteresis Error (*HE*) was computed at each U_s from the following formula:

$$HE(\%) = \frac{Uo\_unloading\ (10N) - Uo\_loading\ (10N)}{Uo(20N)} \cdot 100\% \tag{1}$$

2.3. Drift Characterization

Drift error originates from viscoelastic response of polymers. In order to determine the drift error, the sensors were loaded to a constant force of 15 N for a time span of one hour. Immediately after the application of the force, U_o was registered for all sensors; this measurement was designated as U_o (0h). After one hour, the output voltage was registered again to obtain U_o (1h). With these data, the Drift Error (*DE*) was computed on the percentage basis as follows:

$$DE(\%) = \frac{Uo(1h) - Uo(0h)}{Uo(0h)} \cdot 100\% \tag{2}$$

The aforementioned procedure was repeated at all the input voltages specified in this Section. This let us assess the drift error as a function of U_s.

3. Experimental results and discussion

This section discusses the experimental assessment of sensors' sensitivity, hysteresis and drift errors at multiple input voltages, U_s. Dispersion analysis is embraced for each metric on the basis of the μ/σ quotient where μ and σ are respectively the mean value of the metric and its standard deviation. The rule of thumb when comparing sensors is that the error metric should be as low as possible, and also, dispersion should be held to a minimum. Low dispersion implies a high μ/σ that ultimately yields high part-to-part repeatability.

3.1. Sensitivity results

Figure 4 shows the sensitivity dispersion for the whole set of input voltages and for both sensor brands. In general, there is not a remarkable difference in the dispersion of both brands, but noticeably, the sensitivity dispersion of Interlink sensors exhibits less variation to changes in the input voltage. On the hand, the sensitivity dispersion of Peratech sensors shows jitter when the input voltage is changed. To better understand the jitter phenomenon, we plotted in Fig. 5 sensor sensitivity as a function of U_s for individual sensors. Note that sensitivity increases in a smooth way for the Interlink sensors. This results in a rather invariant μ/σ quotient in Fig. 4. Conversely, some Peratech sensors show step increments in sensitivity for U_s within the range of 5 V to 7 V, (see the arrow marks in the plot). This, in turn, results in a jitter-like response to the dispersion ratio of Fig. 4. The practical implications of jitter are discussed later.
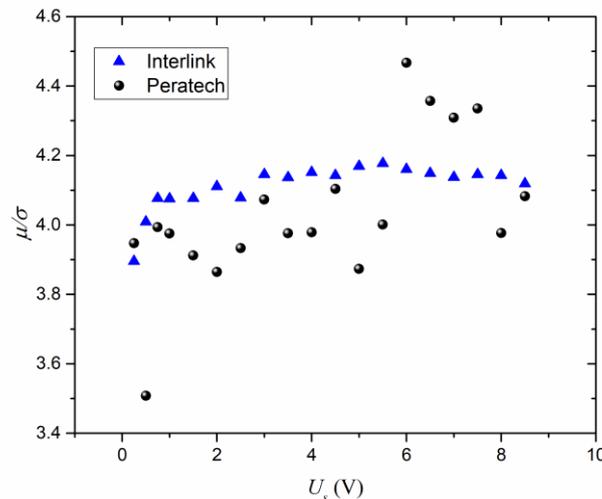

Fig. 4. Dispersion in the sensors' sensitivity as a function of input voltage (U_s). Dispersion calculated from the μ/σ quotient.

On the other hand, the fanning out of sensitivities with incremental U_s may be initially understood as a widening of the sensors' differences with larger input voltages. This observation holds for both sensor brands plotted in Fig. 5. However, by recalling the results of Fig. 4, the following statement can be done: when U_s is increased, the absolute difference in individual sensitivities is enlarged, but on a relative basis the dispersion is held constant. This is so because the standard deviation grows in the same proportion as the mean. From this observation, we can claim that there is not an optimal voltage that minimizes dispersion in sensitivity for the Interlink sensors. Conversely, when Peratech sensors are sourced with 6 V,

there is a maximum in the μ/σ ratio. In practice, this implies that lowest measured dispersion occurs at 6 V, and ultimately, part-to-part repeatability is enhanced.

The underlying phenomena for the jitter behaviour are manifold, but providing an explanation for them falls out of the scope for this article. From the plots in Fig. 5, we can state that this is not an isolated phenomenon as many sensors exhibited the same response.
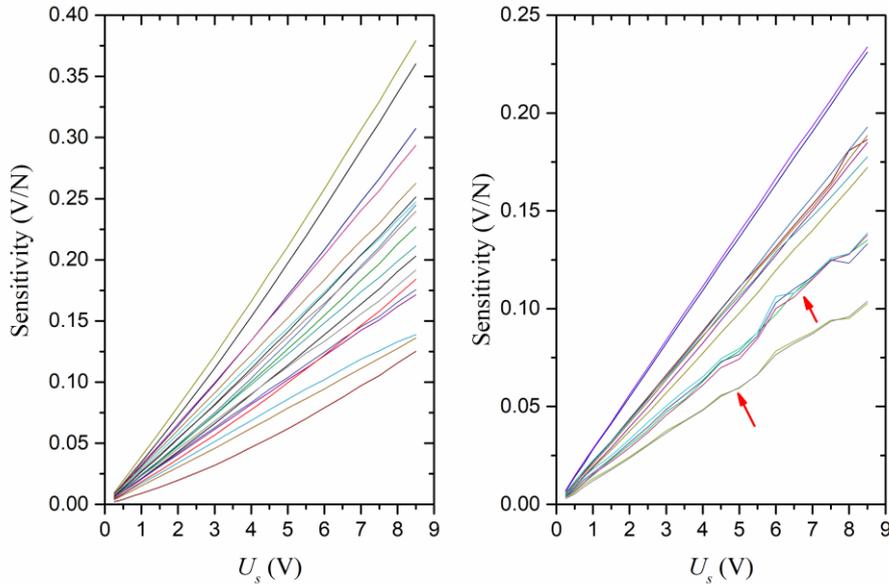

Fig. 5. Sensors' sensitivity as a function of input voltage (U_s) for both sensor brands. Left: Interlink FSR402. Right: Peratech SP200-10. The arrows indicate the step increments in sensitivity for U_s in the range of 5 V to 7 V.

3.2. Hysteresis Error results

The hysteresis error of both sensor brands is shown in Fig. 6; the dispersion in the hysteresis error is shown as well. It is clear from Fig. 6 that the Interlink sensors exhibit a lower hysteresis error for any input voltage. Likewise, it is interesting to note that the *HE* is a voltage-dependent phenomenon as theoretically deducted in a previous work by the authors [31]. From the standpoint of dispersion, it can be noticed from Fig. 6 that the relative dispersion is slightly higher for the Interlink sensor, *i.e.* lower μ/σ means higher dispersion. From a different standpoint, the Peratech sensor exhibits a higher *HE*, but a slightly larger part-to-part repeatability regarding this error metric.

Finally, from the standpoint of the *HE*, there is not a clear best pick, since low error metric and low dispersion are split among both brands. Modelling and compensation of the *HE* is especially useful when dealing with cyclic forces in certain applications, such as gait analysis [34] and footwear design [35].
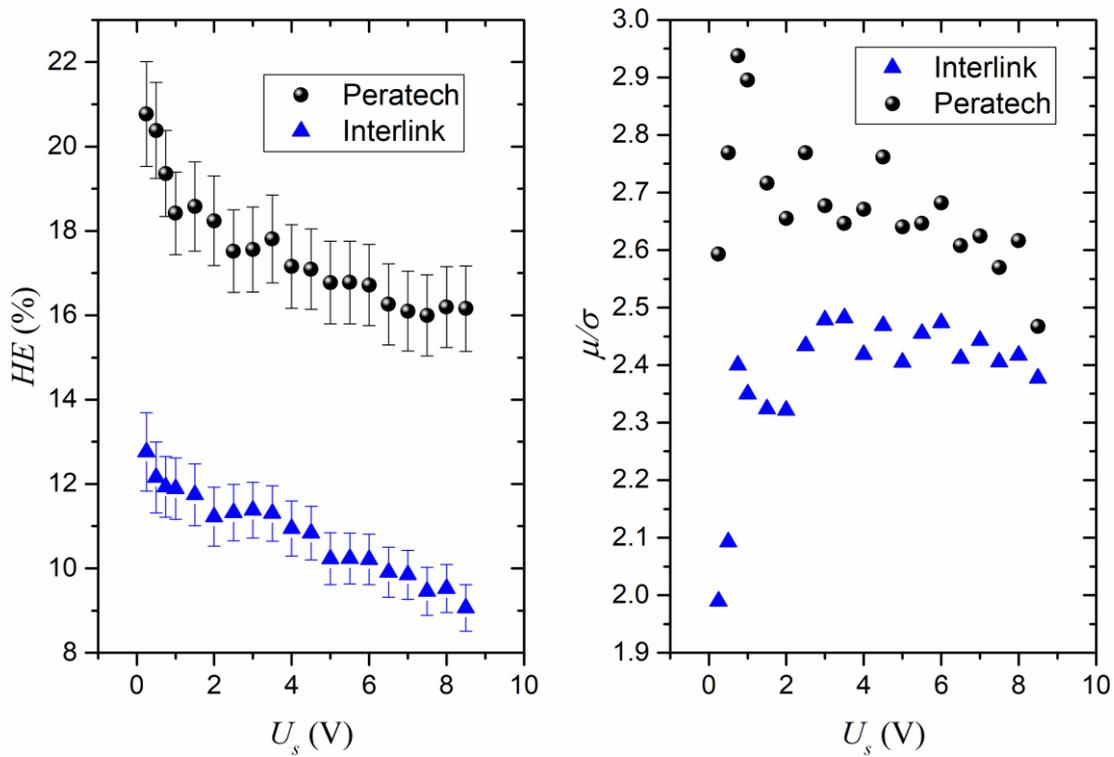
Fig. 6. Hysteresis error (*HE*) as a function of input voltage (U_s). Left: error bar plot comparing the *HE* of both sensor models. Right: dispersion in the *HE* calculated from the μ/σ quotient.

3.3. Drift Error results

The drift error and its dispersion are shown in Fig. 7 for both sensor brands. In this case, the Peratech sensors exhibit a lower *DE* than the Interlink sensors, but a relative higher dispersion. In other words, the electrical resistance of an Interlink sensor drifts more over time when compared with a Peratech sensor, but in general, Interlink sensors exhibit more repeatable drift readings. The practical consequences of the results reported in Fig. 7 are discussed in the next section.

Drift is the major drawback of FSRs that it is currently limiting their extensive usage. Certain implementations that involve application of force over an extended time period require low drift readings that FSRs cannot currently meet. Previous work of the authors had focused on deep understanding of the drift phenomenon of FSRs. It was then found that drift is a voltage-dependent phenomenon [28]. In brief, the larger U_s is, the lower the *DE* results, and therefore, it is advisable to source the FSRs at a high U_s in order to reduce the *DE*. Note that this observation also applies to the *HE* as previously reported in the plot of Fig. 6. However, there is a limit on how big U_s can be without affecting FSRs performance. If U_s is over 7 V, sensors' sensitivity degrades over time [31].
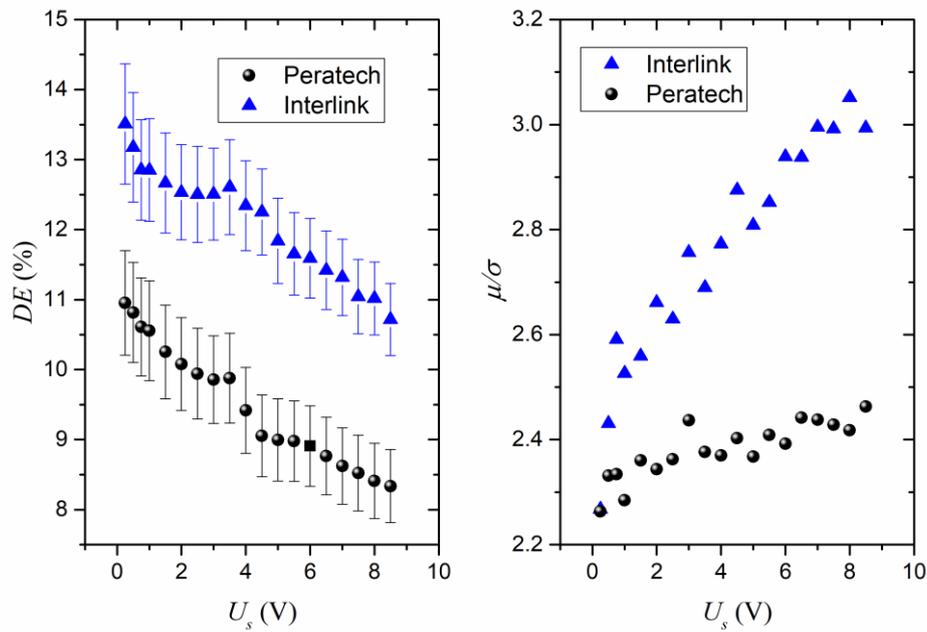
Fig. 7. Drift error (D*E*) as a function of input voltage (U_s). Left: error bar plot comparing the *DE* of both sensor models. Right: dispersion in the *DE* calculated from the quotient μ/σ.

3.4. Discussion of results

In order to provide a meaningful discussion of the experimental results, we must bear in mind two aspects: first, what is the intended final application of the FSRs? And second, what is more important in our final application, the error metric or the part-to-part repeatability?

As previously mentioned, applications with cyclic loading such as gait analysis [34] and footwear design [35], require sensors with the lowest possible hysteresis error. Typically, this kind of applications demands multiple sensors, and therefore, part-to-part repeatability is also desirable. However, poor part-to-part repeatability can be overcome with individual sensor calibration, but this clearly requires additional time and effort that ultimately translates into higher costs.

On the other hand, certain applications incorporate FSRs to distinguish objects by their force profile [36], thus requiring multiple FSRs [37]. In this final application, error metrics of hysteresis and drift are less important, but part-to-part repeatability is clearly more relevant.

A different type of application incorporates FSRs as means of estimating the amount of items in an inventory system [38]. Considering that inventory management requires a continuous measuring over an extended time period, drift error plays a major role in this scenario. However, part-to-part repeatability should be also taken into account because this type of deployment requires multiple sensors, and also, the inventory system must be replicated for every item in the store.

In order to address the initial questions from this section, we must decide whether individual sensor calibration is available or not. If available, metric dispersion is less important, and therefore, a low error metric is the most important factor for picking one brand over another. In this scenario, we may skip error compensation depending on the final application requirements. Conversely, if individual sensor calibration is not possible, it is advisable to pick the sensor model with the lowest dispersion in the error metric of interest, and then provide error compensation via software using global parameters. The definition of

global parameters implies that we compensate for a given error on the basis of an average, *e.g.*, we obtain an average drift error for multiple sensors of a specific brand, and then perform compensation with such information.

4. Conclusions

An automated testbench for characterization of FSRs has been presented. A sandwich-like configuration was employed to handle up to sixteen sensors simultaneously. Similarly, a linear motor with a spring was deployed to apply multiple force profiles to the bunch of sensors. Data collection was possible from a time-multiplexed circuit.

Experimental characterization of sensitivity, hysteresis error and drift error was carried out at multiple input voltages (U_s) for multiple Interlink FSR402 and Peratech SP200-10 sensors. Dispersion in these metrics was assessed by means of the quotient between the mean and the standard deviation. In regard to sensitivity, it was found that the Interlink sensor had rather constant sensitivity dispersion for any input voltage, whereas the Peratech sensor exhibited minimal dispersion at $U_s = 6$ V. Hence; we claim that $U_s = 6$ V is the optimal voltage to maximize part-to-part repeatability in Peratech sensors.

In regard to the hysteresis and drift errors; mixed results were found. The interlink sensors exhibited lower hysteresis error but a comparatively higher dispersion in this metric. On the other hand, the Peratech sensors exhibited lower drift error but a comparatively higher dispersion in this metric. Therefore, there is not the best pick sensor based on these error metrics. Every application must evaluate the pro and cons of using either one brand or another.

Acknowledgements

References

[1] Alotaibi, A., & Anwar, S. (2021). A Fuzzy Logic based piezoresistive/piezoelectric fusion algorithm for carbon nanocomposite wide band strain sensor. *IEEE Access*, *9*, 14752-14764. https://doi.org/10.1109/ACCESS.2020.3049081

[2] Chen, T., Wei, P., Chen, G., Liu, H., Mugaanire, I. T., Hou, K., & Zhu, M. (2021). Heterogeneous structured tough conductive gel fibres for stable and high-performance wearable strain sensors. *Journal of Materials Chemistry A*, *9*(20), 12265-12275. https://doi.org/10.1039/d1ta02422a

[3] Cui, C., Fu, Q., Meng, L., Hao, S., Dai, R., & Yang, J. (2020). Recent progress in natural biopolymers conductive hydrogels for flexible wearable sensors and energy devices: materials, structures, and performance. *ACS Applied Bio Materials*, *4*(1), 85-121. https://doi.org/10.1021/acsabm.0c00807

[4] Liu, Z. Z., Wang, H. P., Yuan, L., Wang, W., Zhang, C., & Xue, Y. (2021). A film stress measurement system applicable for hyperbaric environment and its application in coal and gas outburst simulation test. *Metrology and Measurement Systems*, *28*(1), 73-88. https://doi.org/10.24425/mms.2021.135991

[5] Fernandez, F. D. M., Khadka, R., & Yim, J. H. (2020). Highly porous, soft, and flexible vapor-phase polymerized polypyrrole–styrene–ethylene–butylene–styrene hybrid scaffold as ammonia and strain sensor. *RSC Advances*, *10*(38), 22533-22541. https://doi.org/10.1039/d0ra03592k

[6] Lu, L., Yang, B., & Liu, J. (2020). Flexible multifunctional graphite nanosheet/electrospun-polyamide 66 nanocomposite sensor for ECG, strain, temperature and gas measurements. *Chemical Engineering Journal*, *400*, 125928. https://doi.org/10.1016/j.cej.2020.125928

[7] Shukla, P., & Saxena, P. (2021). Polymer nanocomposites in sensor applications: a review on present trends and future scope. *Chinese Journal of Polymer Science*, *39*(6), 665-691. https://doi.org/10.1007/s10118-021-2553-8

[8] Sharma, S., Sudhakara, P., Omran, A. A. B., Singh, J., & Ilyas, R. A. (2021). Recent trends and developments in conducting polymer nanocomposites for multifunctional applications. *Polymers*, *13*(17), 2898. https://doi.org/10.3390/polym13172898

[9] Idumah, C. I., Ezeani, E. O., & Nwuzor, I. C. (2021). A review: advancements in conductive polymers nanocomposites. *Polymer-Plastics Technology and Materials*, *60*(7), 756-783. https://doi.org/10.1080/25740881.2020.1850783

[10] Ma, Z., Li, H., Jing, X., Liu, Y., & Mi, H. Y. (2021). Recent advancements in self-healing composite elastomers for flexible strain sensors: Materials, healing systems, and features. *Sensors and Actuators A: Physical*, *329*, 112800. https://doi.org/10.1016/j.sna.2021.112800

[11] Chang, S., Li, J., & Liu, H. (2020). Research Progress of Flexible Strain/Pressure Sensors Based on Biomaterial Derived Materials. *Materials Reports, 34*(19), 19173–19182. https://doi.org/10.11896/cldb.19050179 (in Chinese)

[12] Saleh, M. A., Kempers, R., & Melenka, G. W. (2021). A comparative study on the electromechanical properties of 3D-Printed rigid and flexible continuous wire polymer composites for structural health monitoring. *Sensors and Actuators A: Physical*, *328*, 112764. https://doi.org/10.1016/j.sna.2021.112764

[13] Yuan, C. L., & Lin, S. W. (2014). Detection of organic chemical vapors with a MWNTs-polymer array chemiresistive sensor. *Materials Science-Poland*, *32*(1), 50-58. https://doi.org/10.2478/s13536-013-0160-2

[14] Speller, N. C., Siraj, N., McCarter, K. S., Vaughan, S., & Warner, I. M. (2017). QCM virtual sensor array: Vapor identification and molecular weight approximation. *Sensors and Actuators B: Chemical*, *246*, 952-960. https://doi.org/10.1016/j.snb.2017.02.042

[15] Jaffal, D., Daniels, S., Tang, H. Y., Ghadimi, H., & Monty, C. N. (2021). Electroconductive nylon-6/multi-walled carbon nanotube nanocomposite for sodium sensing applications. *Composites Part C: Open Access, 4*, 100116. https://doi.org/10.1016/j.jcomc.2021.100116

[16] Zhao, X., Wang, W., Wang, Z., Wang, J., Huang, T., Dong, J., & Zhang, Q. (2020). Flexible PEDOT: PSS/polyimide aerogels with linearly responsive and stable properties for piezoresistive sensor applications. *Chemical Engineering Journal*, *395*, 125115. https://doi.org/10.1016/j.cej.2020.125115

[17] Lai, H., Zhuo, H., Hu, Y., Shi, G., Chen, Z., Zhong, L., & Zhang, M. (2021). Anisotropic carbon aerogel from cellulose nanofibers featuring highly effective compression stress transfer and pressure sensing. *ACS Sustainable Chemistry & Engineering*, *9*(29), 9761-9769. https://doi.org/10.1021/acssuschemeng.1c02051

[18] Huang, J., Zhao, M., Hao, Y., Li, D., Feng, J., Huang, F., & Wei, Q. (2021). Flexible, Stretchable, and Multifunctional Electrospun Polyurethane Mats with 0D-1D-2D Ternary Nanocomposite-Based Conductive Networks. *Advanced Electronic Materials*, *7*(1), 2000840. https://doi.org/10.1002/aelm.202000840

[19] Tang, X., Pionteck, J., Krause, B., Pötschke, P., & Voit, B. (2021). Highly Tunable Piezoresistive Behavior of Carbon Nanotube-Containing Conductive Polymer Blend Composites Prepared from Two Polymers Exhibiting Crystallization-Induced Phase Separation. *ACS Applied Materials & Interfaces*, *13*(36), 43333-43347. https://doi.org/10.1021/acsami.1c10480

[20] Dai, X., Huang, L. B., Du, Y., Han, J., & Kong, J. (2021). Self-healing flexible strain sensors based on dynamically cross-linked conductive nanocomposites. *Composites Communications*, *24*, 100654. https://doi.org/10.1016/j.coco.2021.100654

[21] Y Fang, Y., Xu, J., Gao, F., Du, X., Du, Z., Cheng, X., & Wang, H. (2021). Self-healable and recyclable polyurethane-polyaniline hydrogel toward flexible strain sensor. *Composites Part B: Engineering*, *219*, 108965. https://doi.org/10.1016/j.compositesb.2021.108965

[22] Hall, R. S., Desmoulin, G. T., & Milner, T. E. (2008). A technique for conditioning and calibrating force-sensing resistors for repeatable and reliable measurement of compressive force. *Journal of Biomechanics*, *41*(16), 3492-3495. http://dx.doi.org/10.1016/j.jbiomech.2008.09.031

[23] Komi, E. R., Roberts, J. R., & Rothberg, S. J. (2007). Evaluation of thin, flexible sensors for time-resolved grip force measurement. *Proceedings of the Institution of Mechanical Engineers, Part C: Journal of Mechanical Engineering Science*, *221*(12), 1687-1699. https://doi.org/10.1243/09544062JMES700

[24] J Dabling, J. G., Filatov, A., & Wheeler, J. W. (2012, August). Static and cyclic performance evaluation of sensors for human interface pressure measurement. *In 2012 Annual International Conference of the IEEE Engineering in Medicine and Biology Society* (pp. 162-165). IEEE. https://doi.org/10.1109/EMBC.2012.6345896

[25] Hollinger, A., & Wanderley, M. M. (2006, June). Evaluation of commercial force-sensing resistors. *In Proceedings of the International Conference on New Interfaces for Musical Expression*, Paris, France (pp. 4-8).

[26] Interlink Electronics. (2017). *FSR400 Series Data Sheet* [Datasheet PDS-10004-C]

[27] Peratech Inc. (2015). *QTC SP200 Series Datasheet. Single Point Sensors* [Datasheet V1.1] https://www.peratech.com/assets/uploads/datasheets/Peratech-QTC-DataSheet-SP200-Series-Nov15.pdf

[28] Cruz-Pacheco, A. F., Paredes-Madrid, L., Orozco, J., Gómez-Cuaspud, J. A., Batista-Rodríguez, C. R., & Palacio Gomez, C. A. (2020). Assessing the influence of the sourcing voltage on polyaniline composites for stress sensing applications. *Polymers*, *12*(5), 1164. https://doi.org/10.3390/polym12051164

[29] Ma, Z., Li, H., Jing, X., Liu, Y., & Mi, H. Y. (2021). Recent advancements in self-healing composite elastomers for flexible strain sensors: Materials, healing systems, and features. *Sensors and Actuators A: Physical*, *329*, 112800. https://doi.org/10.1016/j.sna.2021.112800

[30] Kalantari, M., Dargahi, J., Kövecses, J., Mardasi, M. G., & Nouri, S. (2011). A new approach for modeling piezoresistive force sensors based on semiconductive polymer composites. *IEEE/ASME Transactions on Mechatronics*, *17*(3), 572-581. https://doi.org/10.1109/TMECH.2011.2108664

[31] Paredes-Madrid, L., Matute, A., & Palacio, C. (2019). Understanding the effect of sourcing voltage and driving circuit in the repeatability of measurements in force sensing resistors (FSRs). *Measurement Science and Technology*, *30*(11), 115101. https://doi.org/10.1088/1361-6501/ab3307

[32] Simmons, J. G. (1963). Electric tunnel effect between dissimilar electrodes separated by a thin insulating film. *Journal of Applied Physics*, *34*(9), 2581-2590. http://dx.doi.org/10.1063/1.1729774

[33] Mikrajuddin, A., Shi, F. G., Kim, H. K., & Okuyama, K. (1999). Size-dependent electrical constriction resistance for contacts of arbitrary size: from Sharvin to Holm limits. Materials Science in Semiconductor Processing, 2(4), 321-327. https://doi.org/10.1016/S1369-8001(99)00036-0

[34] Chen, D., Cai, Y., & Huang, M. C. (2018). Customizable pressure sensor array: Design and evaluation. *IEEE Sensors Journal*, *18*(15), 6337-6344. https://doi.org/10.1109/JSEN.2018.2832129

[35] Martínez-Barba, D. A., Martínez-Manuel, R., Daza-Benítez, L., & Vidal-Lesso, A. (2020). Development of self-calibrating sensor footwear and relevance of in-shoe characterization on accurate plantar pressure distribution measurements. *IEEE Sensors Journal*, *21*(6), 8421-8431. https://doi.org/10.1109/JSEN.2020.3048611

[36] J Castellanos-Ramos, J., Navas-González, R., Macicior, H., Sikora, T., Ochoteco, E., & Vidal-Verdú, F. (2010). Tactile sensors based on conductive polymers. *Microsystem Technologies*, *16*(5), 765-776. https://doi.org/10.1007/s00542-009-0958-3

[37] Hidalgo-López, J. A., Oballe-Peinado, Ó., Castellanos-Ramos, J., Sánchez-Durán, J. A., Fernández-Ramos, R., & Vidal-Verdú, F. (2017). High-accuracy readout electronics for piezoresistive tactile sensors. *Sensors*, *17*(11), 2513. https://doi.org/10.3390/s17112513

[38] Lim, R., Choong, D. S. W., & Cheng, M. Y. (2020, December). Development of Pressure Sensing Array System for Retail Inventory Management. *In 2020 IEEE 22nd Electronics Packaging Technology Conference (EPTC)* (pp. 185-188). IEEE. https://doi.org/10.1109/EPTC50525.2020.9315015

Carlos Palacio received the Ph.D. degree in physical sciences from Ghent University, Belgium, in 2008. He has been a full-time professor at Antonio Nariño University since 2013. He has authored or coauthored 1 book chapter, and over 30 journal publications. He is a member of the editorial board in an international journal and has been reviewer of several papers in international journals. His current research interests include solid state physics, materials characterization, new materials, nano-science and the study of force-sensors.

Andrés Garzón received his B.Sc. degree in automation engineering from La Salle University, Bogotá, Colombia, in 2011, the M.Scc degree in materials & manufacturing engineering and the Ph.D. degree in material science from the National University of Colombia, in 2020. He has been a research assistant in materials and surfaces at University of Málaga, Spain. He has been a full-time professor at Universidad Católica de Colombia since 2021. His research interests are instrumentation and control of autonomous systems.

Leonel Paredes-Madrid w received his B.Sc. degree in electronic engineering from Simon Bolivar University, Caracas, Venezuela, in 2007 and the Ph.D. degree in system engineering and automation from Complutense University of Madrid, Spain, in 2014.
He was a research assistant in the Centre for Automation and Robotics CSIC, Madrid, Spain and in Northwestern University, Evanston, Il. He has been a full-time professor at Universidad Católica de Colombia since 2021. His research interests are instrumentation and control of autonomous systems.